Published in final edited form as:
J Am Chem Soc. 2013 July 17; 135(28): 10198–10201. doi:10.1021/ja402645y.

Sc^{3+}-triggered oxoiron(IV) formation from O_2 and its nonheme iron(II) precursor via a Sc^{3+}–peroxo-Fe^{3+} intermediate

Feifei Li[1,&], **Katherine M. Van Heuvelen**[1,#], **Katlyn K. Meier**[2], **Eckard Münck**[2,*], and **Lawrence Que Jr.**[1,*]

[(1)]Department of Chemistry and Center for Metals in Biocatalysis, University of Minnesota, Minneapolis, MN 55455

[(2)]Department of Chemistry, Carnegie Mellon University, Pittsburgh, PA 15213

Abstract

We report that redox-inactive Sc^{3+} can trigger O2 activation by the Fe^{II}(TMC) center (TMC = tetramethylcyclam) to generate the corresponding oxoiron(IV) complex in the presence of BPh_4^- as an electron donor. To model a possible intermediate in the above reaction, we generated an unprecedented Sc^{3+}-adduct of $[Fe^{III}(\eta^2\text{-}O_2)(TMC)]^+$, which was characterized to have an Fe^{III}-(μ-η^2:η^2-peroxo)-Sc^{3+} core and found to convert to the oxoiron(IV) complex. These results have important implications for the role a Lewis acid can play in facilitating O–O bond cleavage during the course of O_2 activation at nonheme iron centers.

There is much current interest in investigating the ability of redox-inactive metal ions to modulate redox reactions by virtue of their Lewis acidity, particularly with respect to their possible roles in O_2 evolution[1] and activation.[2,3] For example, the oxygen-evolving complex of Photosystem II requires a redox-inactive Ca^{2+} ion to produce O_2.[1] In addition, redox-inactive ions have been found to affect the stability and reactivities of high-valent metal-oxo complexes in biomimetic systems[2] as well as to accelerate O_2 activation by Fe^{II} and Mn^{II} complexes.[3] For the latter, heterobimetallic O_2 adducts and high-valent metal-oxo species are presumably involved but have not been observed. We previously demonstrated that $[Fe^{II}(TMC)(NCCH_3)]^{2+}$ (**1**) (TMC = 1,4,8,11-tetramethylcyclam) reacts with O_2 in CH_3CN in the presence of stoichiometric H^+ and BPh_4^- to form $[Fe^{IV}O(TMC)(NCCH_3)]^{2+}$ (**4**).[4] Herein, we report that a redox-inactive Sc^{3+} ion can replace the strong acid in this reaction to *trigger* the formation of **4**. An unprecedented Sc^{3+} adduct (**3**) of $[Fe^{III}(\eta^2\text{-}O_2)(TMC)]^+$ (**2**) was trapped, spectroscopically characterized in detail, and found to convert to **4** (Scheme 1).

Complex **1** is air stable in acetonitrile solution for days. However, the addition of 1 equiv. $Sc(OTf)_3$ together with 1 equiv. $NaBPh_4$ to an aerobic solution of **1** resulted in the formation of **4** in >70% yield over the course of ~1 h at 0 °C, as indicated by its signature near-IR band at 820 nm (Figure 1A).[5] Electrospray ionization mass spectra of the solution revealed the evolution of a prominent peak at m/Z = 477.0, assigned to the $\{[Fe^{IV}(O)(TMC)](OTf)\}^+$ ion based on its position and isotope distribution pattern (Figure S1). When the reaction was carried out with $^{18}O_2$, the *m/Z* = 477 peak showed an upshift of 2 units (Figure S2),

[*]**Corresponding Authors**emunck@cmu.edu. larryque@umn.edu. .
[&]**Present Addresses** Brookhaven National Laboratory, Upton, NY 11973
[#]**Present Addresses** Harvey Mudd College, Claremont, CA 91711

ASSOCIATED CONTENT Supporting Information. Syntheses, physical methods, ESI-MS, ^{1}H NMR, and XANES figures, and details of XANES and XAS analysis are in the SI, which is available free of charge via the Internet at http://pubs.acs.org.

confirming that the oxo moiety of **4** derived from dioxygen *and* that O–O bond cleavage must occur for the formation of **4** from **1** and O_2.

Further investigation demonstrated the requirement for both Sc^{3+} and BPh_4^- for the formation of **4** from **1**, as addition of either BPh_4^- or Sc^{3+} alone to **1** in air-saturated CH_3CN solution did not elicit any detectable change in the UV-visible spectra. In addition, the yield of **4** correlated linearly with the amount of BPh_4^- added, plateauing at 1.0 equiv. BPh_4^- (Figure 1B). ^{1}H-NMR studies of the final solution showed that BPh_4^- had decomposed to 1,1′-biphenyl (Figure S3) with a stoichiometry of 0.95±0.15 equiv. relative to **1**, demonstrating that BPh_4^- provides the two electrons needed to convert **1** and O_2 into **4**. On the other hand, a sub-stoichiometric amount of Sc^{3+} was sufficient for the maximal formation of **4** (Figure 1B inset), suggesting that Sc^{3+} can act somewhat 'catalytically'.

As shown in Figure 1A, no intermediates are evident in the UV-Vis spectra during the conversion of **1** to **4**.[6] To account for the role of Sc^{3+} in this transformation, we propose the formation of a Sc^{3+}-peroxo-Fe^{3+} adduct that is reminiscent of the Fe^{III}–OOH species proposed in the H^+-and-BPh_4^--promoted generation of **4** from O_2 and **1**.[4,7] To test this hypothesis, $Sc(OTf)_3$ was added to a solution of the blue $Fe^{III}(\eta\text{-}O_2)$ complex **2** (purified via precipitation as its BPh_4 salt; see SI for details), which resulted in the immediate generation of a magenta intermediate (**3**) and its subsequent conversion to **4** in ~70% yield over the course of ~1 h at −10 °C (Figure 2A).

What is the identity of **3**? Complex **3** exhibits a λ_{max} of 520 nm (ε_{520} = 780 $M^{-1}cm^{-1}$) established from its UV-visible spectrum (Figure 2A) and Mössbauer analysis. The large blue shift observed for the peroxo-to-Fe(III) charge transfer band of **2** (λ_{max} 835 nm) is reminisent of that seen upon protonation of **2** to form $[Fe^{III}(TMC)(\eta^1\text{-}OOH)]^{2+}$ in CH_3CN (**5**),[7a] indicating partial neutralization of the negative charge of the peroxo ligand. Titration of **2** with $Sc(OTf)_3$ showed that 1 equiv $Sc(OTf)_3$ was nearly sufficient to cause the 835-nm band of **2** to disappear, suggesting a 1:1 stoichiometry for the Sc^{3+}-adduct of **2** (Figure 2B). The EPR spectrum of **3** shows features at g = 9.1, 5.1, 3.6 and ~2, consistent with an S = 5/2 iron(III) center with an E/D of 0.18 (Figure 3 left), compared to E/D values of 0.28 and 0.097 for **2** and **5**,[7a] respectively. The Mössbauer spectra of **3** (Figure 3 right) are typical of high-spin iron(III); their analysis is described in the SI and Mössbauer parameters are listed in Table 1 and Figure 3 caption. A comparison of the spectroscopic properties in Table 1 shows that **3** is quite different from **2** and **5**, indicating that Sc^{3+} significantly affects the properties of the peroxoiron(III) unit.

We also carried out Fe K-edge X-ray absorption spectroscopic (XAS) studies to investigate the structural features of **3**. Complex **3** exhibits an Fe K-edge at 7125.3 eV and a pre-edge feature at 7113.3 eV, which are comparable to those of **2** and **5** obtained in CH_3CN solvent (Figure S4, Table S1).[7a] The pre-edge feature of **3** has an area of 14.4(6) units, compared to 17.9 for **2** and 22.4 for **5** (Table S1). As the pre-edge area reflects the extent to which the iron center deviates from centrosymmetry, the coordination environment of **3** must be closer to that of **2** with an η^2-peroxo ligand than that of **5** with an η^1-OOH ligand.

Analysis of the EXAFS data of **3** provides additional structural insight. Best fits reveal 4 N scatterers at 2.18 Å and 4 C scatterers each at 3.00 and 3.15 Å; all these features arise from the TMC ligand and have distances close to those found for **2** (Figure 4, Table S2). In addition, there is an O subshell at 1.98(1) Å arising from the peroxo ligand. Notably, the Fe–O distance of **3** is significantly longer than the 1.91-Å distance found for **2**,[7a] implying the addition of Sc^{3+} significantly weakens the iron-peroxo interaction. This 0.07-Å lengthening is inconsistent with conversion of the η^2-peroxo ligand to an η^1-isomer, as related η^1-peroxo complexes **5** and **6** both have shorter Fe–O distances (Table 2). Cu^{II} adducts to (η^2-

peroxo)heme complexes also have one short Fe–O bond of ~1.93 Å in a highly unsymmetric η^2-peroxo ligand that binds to the iron.[9] Thus, the 0.07-Å lengthening of the *r*(Fe–O) of **3** relative to that of **2** favors a symmetric η^2-peroxo binding mode for **3**. This conclusion is also supported by a comparison of fits 7 and 8 in Table S2, where the 2-O subshell in fit 7 has a σ^2 value of ~4, while the 1-O subshell in fit 8 has a σ^2 value of −0.4. A negative σ^2 value for the latter indicates that either a bond is more rigid than would be expected for its distance or that there are too few scatterers associated with that shell.[10] A negative σ^2 value was also found when only one O-scatterer (instead of two) was used in fitting the EXAFS data for **2**. Our EXAFS results thus demonstrate that the binding of Sc^{3+} retains the symmetric side-on binding mode of the peroxo ligand in **3** but elongates the *r*(Fe–O) by 0.07 Å.[11]

The final key piece of evidence for the identity of **3** comes from resonance Raman spectroscopy. Laser excitation into the intense 520-nm band of **3** reveals two prominent peaks at 807 and 543 cm^{-1} (Figure 5) that correspond to ν(O–O) and ν(Fe–O) modes, respectively. These assignments are corroborated by ^{18}O-labeling, resulting in respective downshifts of 45 and 23 cm^{-1} that correlate well with Hooke's Law predictions for these modes and support the presence of an iron-bound peroxo ligand in **3**.[12] The ν(O–O) of **3** is the lowest of any nonheme high-spin peroxoiron(III) complex thus far observed (Table 2). Relative to its precursor **2**,[7a] **3** has a ν(O–O) that is downshifted by 19 cm^{-1} and a ν(Fe–O) that is upshifted by 50 cm^{-1}, consistent with the retention of the η^2 binding mode of the peroxo ligand. Taken together, the spectrosopic data lead us to propose a $Fe^{3+}(\mu\text{-}\eta^2\text{:}\eta^2\text{-O})Sc^{3+}$ core for **3**, analogous to the $Ni^{2+}(\mu\text{-}\eta^2\text{:}\eta^2\text{-}O_2)K^+$ core found in a complex characterized crystallographically by Limberg, Driess, and coworkers.[13,14] With the nature of **3** characterized, an important question that remains is whether it is involved in the conversion of **1** to **4** by O_2 activation. The requirement for both Sc^{3+} and two electrons to trigger O_2 activation of **1** suggests the likely formation of a Sc^{3+}-peroxo-Fe^{3+} species like **3** as an intermediate (Scheme 1). However the fact that this species does not accumulate during O_2 activation (Figure 1A) suggests that **3** may correspond to a more stable isomer of the actual intermediate involved in the O_2 activation reaction. Nevertheless, **3** represents a rare example of a heterobimetallic complex bridged by a peroxo ligand[9,13] and the only one thus far involving a nonheme iron center.

The spectroscopic characterization of **3** as a complex with an $Fe^{3+}(\mu\text{-}\eta^2\text{:}\eta^2\text{-}O_2)Sc^{3+}$ core provides a plausible mechanism for a Lewis acid to promote O–O bond cleavage. This insight points to another role the second iron center can play in diiron enzymes besides serving as an electron source: functioning as a Lewis acid to facilitate formation of high-valent iron-oxo intermediates such as **Q** and **X** in the respective oxygen activating cycles of methane monooxygenase and Class 1A ribonucleotide reductases.[18] This report of the Sc^{3+}-peroxo-Fe^{3+} intermediate (**3**) also augments the recent literature focused on the effects of redox-inactive Lewis acidic metal ions on redox transformations.[1,2,3] Prominent among these are their accelerative properties in oxidations by high-valent metal-oxo complexes discovered by Fukuzumi and Nam[2a-f] as well as the role of Ca^{2+} in forming an O–O bond from water during photosynthesis.[1] Relevant to the latter, Borovik recently showed that group II metal ions (M^{II}) can enhance the rates of O_2 activation by Fe^{II} and Mn^{II} complexes to afford well characterized M^{II}–(μ-OH)–(Mn^{III}/Fe^{III}) products, presumably via heterobimetallic O_2 adducts.[3] Our results herein demonstrate that Sc^{3+} can turn "on" the activation of O_2 at a nonheme iron center *and* that a transient Sc^{3+}–peroxo–Fe^{3+} species related to **3** could be a viable intermediate leading to O–O bond cleavage.

Supplementary Material

Refer to Web version on PubMed Central for supplementary material.

Acknowledgments

Funding Sources This work was supported by the National Science Foundation (grant CHE1058248 to L.Q.) and the National Institutes of Health (grant EB001475 to E.M. and postdoctoral fellowship GM093479 to K.M.V.H.). F.L. acknowledges a doctoral dissertation fellowship from the University of Minnesota. XAS data were collected at beamline X3B of the National Synchrotron Light Source at the Brookhaven National Laboratory and beamline 7-3 of the Stanford Synchrotron Radiation Lightsource, both supported by NIH and DOE.

ABBREVIATIONS

EXAFS	extended X-ray absorption fine structure
TMC	1,4,8,11-tetramethylcyclam
TMCS	1-(2-mercaptoethyl)-4,8,11-trimethyl-1,4,8,11-tetraazacyclotetradecane
XAS	X-ray absorption spectroscopy.

REFERENCES

(1) (a). Yocum CF. Coord. Chem. Rev. 2008; 252:296–305.(b) Umena Y, Kawakami K, Shen J-R, Kamiya N. Nature. 2011; 473:55–60. [PubMed: 21499260] (c) Tsui E,Y, Tran R, Yano J, Agapie T. Nature Chem. 2013; 5:293–299. [PubMed: 23511417]

(2) (a). Fukuzumi S. Coord. Chem. Rev. 2013; 257:1564–1575.(b) Fukuzumi S, Morimoto Y, Kotani H, Naumov P, Lee Y-M, Nam W. Nature Chem. 2010; 2:756–759. [PubMed: 20729896] (c) Morimoto Y, Kotani H, Park J, Lee Y-M, Nam W, Fukuzumi S. J. Am. Chem. Soc. 2011; 133:403–405. [PubMed: 21158434] (d) Park J, Morimoto Y, Lee Y-M, Nam W, Fukuzumi S. J. Am. Chem. Soc. 2011; 133:5236–5239. [PubMed: 21410258] (e) Morimoto Y, Kotani H, Park J, Lee Y-M, Nam W, Fukuzumi S. J. Am. Chem. Soc. 2011; 133:403–405. [PubMed: 21158434] (f) Chen J, Lee Y-M, Davis KM, Wu X, Seo MS, Cho K-B, Yoon H, Park YJ, Fukuzumi S, Pushkar YN, Nam W. J. Am. Chem. Soc. 2013; 135:6388–6391. [PubMed: 23324100] (g) Leeladee P, Baglia RA, Prokop KA, Latifi R, de Visser SP, Goldberg DP. J. Am. Chem. Soc. 2012; 134:10397–10400. [PubMed: 22667991]

(3) (a). Park YJ, Ziller JW, Borovik AS. J. Am. Chem. Soc. 2011; 133:9258–9261. [PubMed: 21595481] (b) Park YJ, Cook SA, Sickerman NS, Sano Y, Ziller JW, Borovik AS. Chem. Sci. 2013; 4:717–726.

(4). Thibon A, England J, Martinho M, Young VG Jr. Frisch JR, Guillot R, Girerd J-J, Münck E, Que L Jr. Banse F. Angew. Chem. Int. Ed. 2008; 47:7064–7067.

(5). Rohde J-U, In J-H, Lim MH, Brennessel WW, Bukowski MR, Stubna A, Münck E, Nam W, Que L Jr. Science. 2003; 299:1037–1039. [PubMed: 12586936]

(6). No intermediates were observed as well in the previously reported reactions of **1** and O_2 to form **4**, irrespective of whether it was promoted by H^+/BPh_4^-,[4] NADH analogs (Hong S, Lee Y-M, Shin W, Fukuzumi S, Nam W. J. Am. Chem. Soc. 2009; 131:13910–13911. [PubMed: 19746912]), or cycloalkene (Lee Y-M, Hong S, Morimoto Y, Shin W, Fukuzumi S, Nam W. J. Am. Chem. Soc. 2010; 132:10668–10670. [PubMed: 20681694]).

(7) (a). Li F, Meier KK, Cranswick MA, Chakrabarti M, Van Heuvelen KM, Münck E, Que L Jr. J. Am. Chem. Soc. 2011; 133:7256–7259. [PubMed: 21517091] (b) Cho J, Jeon S, Wilson SA, Liu LV, Kang EA, Braymer JJ, Lim MH, Hedman B, Hodgson KO, Valentine JS, Solomon EI, Nam W. Nature. 2011; 478:502–505. [PubMed: 22031443] (c) Liu LV, Hong S, Cho J, Nam W, Solomon EI. J. Am. Chem. Soc. 2013; 135:3286–3299. [PubMed: 23368958]

(8). We had difficulties obtaining simulations that simultaneously fit the 0.5 and 8.0 T. spectra. We suspect that the Hamiltonian requires the introduction of quartic terms as we found for **2**.[7a]

(9) (a). Halime Z, Kieber-Emmons MT, Qayyum MF, Mondal B, Gandhi T, Puiu SC, Chufán EE, Sarjeant AAN, Hodgson KO, Hedman B, Solomon EI, Karlin KD. Inorg. Chem. 2010; 49:3629–3645. [PubMed: 20380465] (b) Chufán EE, Puiu SC, Karlin KD. Acc. Chem. Res. 2007; 40:563–572. [PubMed: 17550225] (c) Chishiro T, Shimazaki Y, Tani F, Tachi Y, Naruta Y, Karasawa S, Hayami S, Maeda Y. Angew. Chem. Int. Ed. 2003; 42:2788–2791.

(10). Scott, RA. Physical Methods in Bioinorganic Chemistry. Spectroscopy and Magnetism. Que, L., Jr., editor. University Science Books; Sausalito, CA: 2000. p. 465-503.

(11). We attempted to include in fits of **3** a Sc scatterer at ~3.7 Å. Fits 13 and 14 in Table S2 show that a Sc scatterer of 3.8 Å with a reasonable Debye-Waller factor ($\sigma^2 \sim 4$) can be added, but only a slight improvement in GOF was obtained. Similar results were obtained in the EXAFS analysis of a Sc-O-Co complex (Pfaff FF, Kundu S, Risch M, Pandian S, Heims F, Pryjomska-Ray I, Haack P, Metzinger R, Bill E, Dau H, Comba P, Ray K. Angew. Chem. Int. Ed. 2011; 50:1711–1715.).

(12). At first glance, the 50 cm^{-1} upshift of the Fe–O vibration from **2** to **3** may appear to contradict the observed lengthening of the Fe–O bond distance deduced from EXAFS analysis, but the 18O shifts found for the respective Fe–O vibrations are quite different (−15 vs −23 cm^{-1}). The downshift for **3** is as calculated for a diatomic Fe–O oscillator, but the smaller shift for 2 indicates mixing of the diatomic Fe–O vibration with other vibrational modes. Thus a direct comparison of the frequencies to deduce Fe–O bond distance is not valid in this case.

(13). Yao S, Xiong Y, Vogt M, Grützmacher H, Herwig C, Limberg C, Driess M. Angew. Chem. Int. Ed. 2009; 48:8107–8110.

(14). A related Fe3+(μ-η^2:η^2-O_2)H+ core was postulated by Nam for a short-lived (<2 ms) species (λ_{max} 527 nm) observed at −40 °C upon treatment of **2** with strong acid in its conversion to **5**.[7b]

(15) (a). Girerd J-J, Banse F, Simaan A. J. Struct. Bonding. 2000; 97:145–177.(b) Roelfes G, Vrajmasu V, Chen K, Ho RYN, Rohde J-U, Zondervan C, la Crois RM, Schudde EP, Lutz M, Spek AL, Hage R, Feringa BL, Münck E, Que L Jr. Inorg. Chem. 2003; 42:2639–2653. [PubMed: 12691572] (c) Simaan AJ, Döpner S, Banse F, Bourcier S, Bouchoux G, Boussac A, Hildebrandt P, Girerd J-J. Eur. J. Inorg. Chem. 2000:1627–1633.(d) Neese F, Solomon EI. J. Am. Chem. Soc. 1998; 120:12829–12848.

(16) (a). Brunold TC, Solomon EI. J. Am. Chem. Soc. 1999; 121:8288–8295.(b) Wada A, Ogo S, Nagatomo S, Kitagawa T, Watanabe Y, Jitsukawa K, Masuda H. Inorg. Chem. 2002; 41:616–618. [PubMed: 11849054] (c) Kitagawa T, Dey A, Lugo-Mas P, Benedict JB, Kaminsky W, Solomon E, Kovacs JA. J. Am. Chem. Soc. 2006; 128:14448–14449. [PubMed: 17090014] (d) Katona G, Carpentier P, Nivière V, Amara P, Adam V, Ohana J, Tsanov N, Bourgeois D. Science. 2007; 316:449–453. [PubMed: 17446401]

(17). McDonald AR, Van Heuvelen KM, Guo Y, Li F, Bominaar EL, Münck E, Que L Jr. Angew. Chem. Int. Ed. 2012; 51:9132–9136.

(18) (a). Tinberg CE, Lippard S. J. Acc. Chem. Res. 2011; 44:280–288.(b) Stubbe J, Nocera DG, Yee CS, Chang MCY. Chem. Rev. 2003; 103:2167–2201. [PubMed: 12797828]

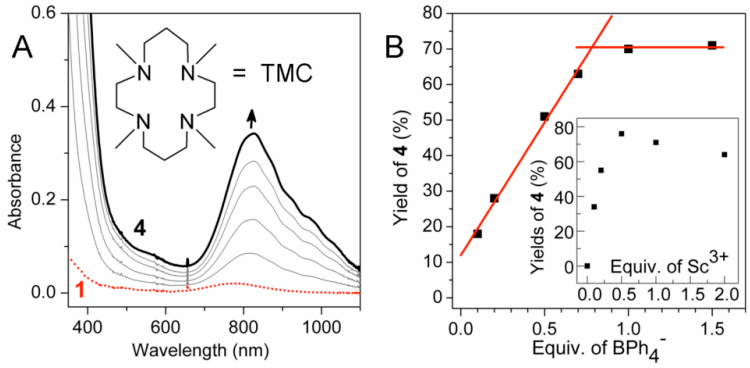

Figure 1.

Reaction of 0.96 mM **1** with NaBPh4 and Sc(OTf)3 in aerobic CH3CN at 0 °C. (**A**) UV-visible spectral changes observed with 1 equiv. NaBPh4 and 1 equiv. Sc(OTf)3. Inset: TMC ligand. (**B**) Plot of the yield of **4** vs. equiv. BPh_4^- in the presence of 1 equiv. Sc^{3+}. Inset: plot of the yield of **4** vs. equiv. of Sc^{3+} with 1 equiv. BPh_4^-.

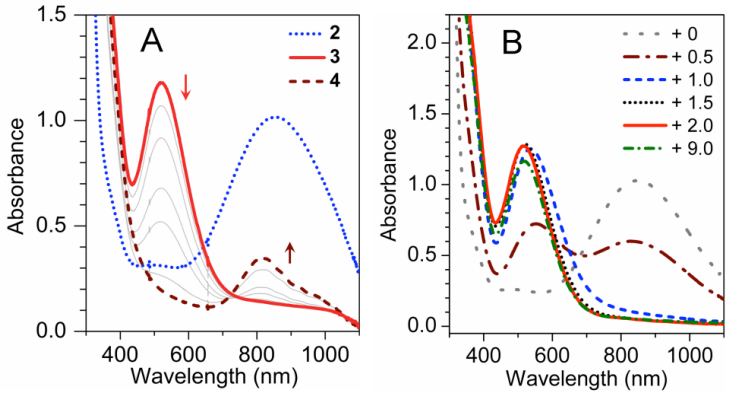

Figure 2.

(**A**) UV-visible spectral changes upon addition of 3 equiv. Sc^{3+} to 1.5 mM *purified* **2** (ε835 = 650 $M^{-1}cm^{-1}$) in CH_3CN at −10 °C instantly generating **3** (ε520 = 780 $M^{-1}cm^{-1}$), which in turn decayed to **4**. (**B**) UV-visible changes upon titration of 1.5 mM **2** in CH3CN at −40 °C with Sc^{3+} (0, 0.5, 1.0, 1.5, 2.0, 9.0 equiv, respectively).

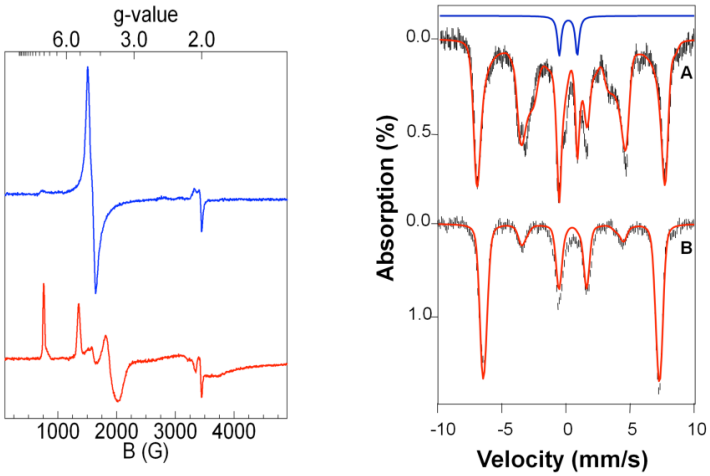

Figure 3.

Left panel: EPR spectra of **2** (blue line, top)[7a] and **3** (red line, bottom) at 2 K and 0.2 mW microwave power. **Right panel**: 4.2 K Mössbauer spectra of **3** in MeCN recorded in parallel applied fields of 0.5 T (A) and 8.0 T (B). The red lines in (A) and (B) are theoretical curves based on eq 1 of the SI, using the following parameters: $D = +1.3\ cm^{-1}$, $E/D = 0.18$, g0 = 2.00, Ax/gnβn = −20.0T, Ax/gnβn = −20.6 T Ax/gnβn = −19.9 T , ΔEQ = 0.50 mm/s, η = −0.5, δ = 0.47 mm/s. The Mössbauer sample contained 90% **3**[8] and 10% Fe^{IV}=O species (blue line).

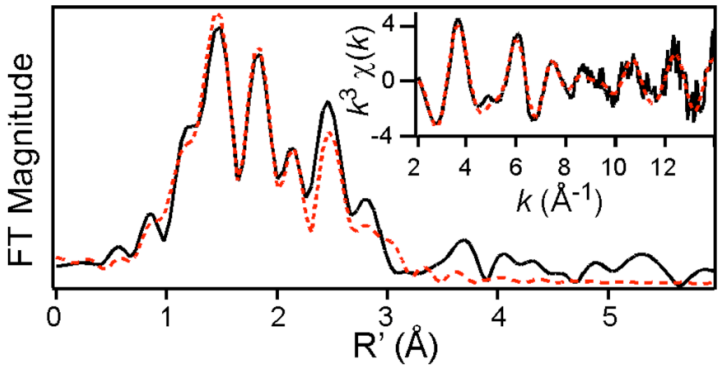

Figure 4.

Fourier transform of Fe K-edge EXAFS data for **3** over a *k*-range of 2-14 Å^{-1}, with $k^3\chi(k)$ vs *k* data shown in the inset. The solid black lines represent the experimental data, while the red dashed lines correspond to the best fit with 2 O @ 1.98 Å and 4 N @ 2.18 Å (fit #22 in Table S3).

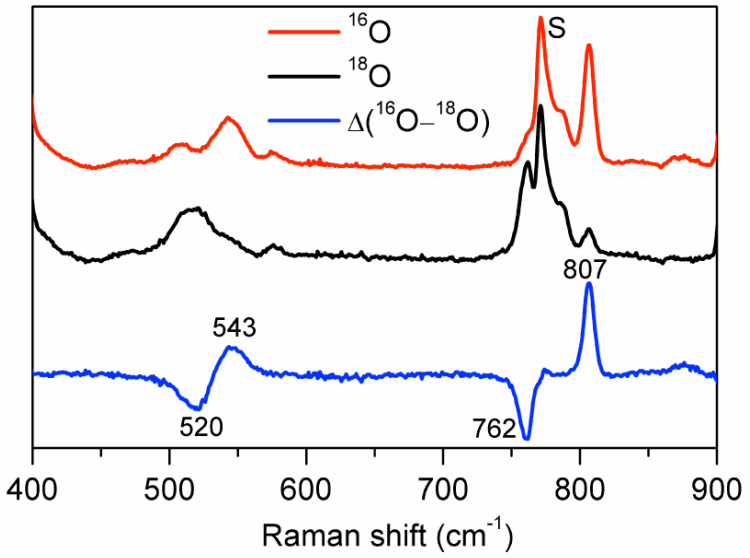

Figure 5.

Resonance Raman spectra of **3** prepared in CH_3CN with $H_2{}^{16}O_2$ (red, top) and $H_2{}^{18}O_2$ (black, middle) obtained with 514.5 nm excitation, 100 mW. The ^{16}O – ^{18}O difference spectrum is shown in blue (bottom). S = solvent.

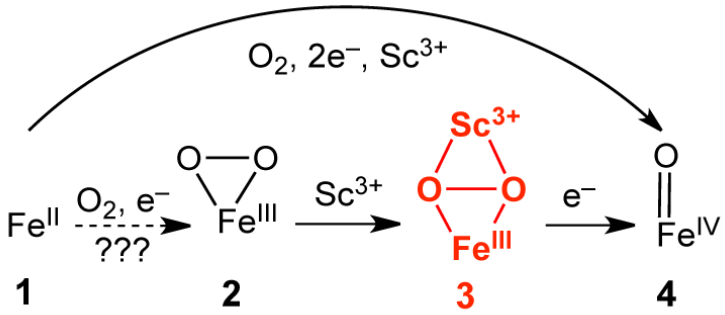

Scheme 1.
Proposed mechanism for the formation of 4 from 1 and O_2

Table 1

Spectroscopic comparison of Fe^{III}(TMC)-peroxo complexes ($S = 5/2$) in CH_3CN

	λ_{max}, nm	ΔEQ, mm/s	δ, mm/s	D, cm^{-1}	E/D	Pre-edge area	ref
2	835	−0.92	0.58	−0.91	0.28	17.9	7a
3	520	0.50	0.47	1.3	0.18	14.4	*
5	500	0.20	0.51	2.5	0.097	22.4	7a

* this work.

Table 2

Comparison of Structural and Raman data for S = 5/2 Fe^{III}-peroxo complexes.

Complexes	*r*(Fe–N) (Å)	*r*(Fe–O) (Å)	ν(O–O) (cm−1)	Ref.
3 #	2.18	1.98, 1.98	807	*
nonheme Fe^{III}-η^2-peroxo			816–827	7, 15
2 (**2′**)#	2.20 (2.21)	1.91, 1.91 (1.91, 1.91)	826 (825)	7a (7b)
nonheme Fe^{III}-η^1-peroxo			830–891	7, 16&
5 (**5′**)#	2.15 (2.16)	1.92 (1.85)	870 (868)	7a (7b)
6$	2.17	1.89		17
(heme)Fe^{III}-(μ-η^2:η^1-O_2)Cu^{II}	2.09	1.92, 2.09	788–808	9a, 9b
(heme)Fe^{III}-(μ-η^2:η^2-O_2)Cu^{II}	2.09	1.94, 2.09	747–767	9a, 9b

#**2, 3**, and **5** in CH_3CN; **2′** and **5′** in a 3:1 (v:v) mixture of acetone:CF_3CH_2OH.

*This work. & See also Table S4 of ref 7a; $ **6** = [Fe^{III}(TMCS)(η^1-O_2)].